Geospatial-Based Assessment of Land Susceptibility Mapping using the Bivariate Statistical Frequency Ratio Model: A Case Study of Idukki District, Kerala, India

Chitikela N. Vara Laxmi* and Kollipara Padma Kumari
School of Spatial Information Technology, IST, JNTUK, Kakinada, Andhra Pradesh, 533003, INDIA
*lakshmichitikela@gmail.com

Abstract

Landslides are one of the most hazardous threats worldwide, posing significant geo-environmental challenges including loss of life, destruction of infrastructure, damage to properties, degradation of agricultural lands and impacting human society. An attempt has been made to prepare the Landslide Susceptibility Zonation (LSZ) map with the help of nineteen geospatial thematic layers using the Geospatial Frequency Ratio (GSFR) model at Idukki district of Kerala, India. The landslide inventory dataset of 1,850 landslide points was identified from historical records (NASA-Co-operative Open Online Landslide Repository (COOLR) and Google Earth dataset divided into training (1,295-70%) and testing (555-30%).

The inventory data and landslide conditioning parameters are used to establish a prediction model of landslide susceptibility. The results showed that 6.22% of the district area falls under very high susceptibility while 17.9 % is categorised as having high susceptibility. Receiver operating characteristic curve (ROC) and area under the curve (AUC) are used to validate the success rate and prediction rate of landslide susceptibility. The FR model achieved the accuracy with a success rate of 0.827 and a prediction rate of 0.835 in the current study.

Keywords: Landslide susceptibility, Geospatial Frequency Ratio model, Landslide inventory, ROC-AUC.

Introduction

Landslides are recurring geophysical disasters, particularly in hilly regions, causing significant damage to landscapes and the environment[15]. These events can be triggered by natural and human-induced factors such as extreme rainfall, heavy winds, earthquakes, floods, volcanic eruptions, construction along slopes, mining activities and debris flows[27]. Landslides are a global issue and not confined to specific regions or Nations. In India, the National Disaster Management Authority (NDMA), a central government organization, has identified landslide-prone areas, particularly in the plateau margins of the Western Ghats and parts of the Eastern Ghats, encompassing the States of Karnataka, Tamil Nadu, Kerala and Maharashtra. Kerala, particularly in the Western Ghats, features hilly terrain with steep slopes and fragile geological formations, making it inherently susceptible to landslides.

The heightened susceptibility arises from a combination of natural factors and human-induced activities[21]. A 2024 study by the World Weather Attribution group revealed that human-induced climate change has amplified the intensity of Kerala's heavy rains by approximately 10%, significantly increasing the likelihood of landslides.

Additionally, human activities such as deforestation, unplanned construction and quarrying exacerbate the risks, further destabilizing the region's delicate landscape. The assessment of deforestation and landscape details through physical surveys and manual preparations can be time-consuming and labour-intensive. To address these challenges, the integration of remote sensing and GIS tools within geospatial technologies offers a comprehensive and efficient approach, delivering valuable information to planners and managers for effective decision-making.

Analysing the spatial and temporal changes caused by human activities such as deforestation, overgrazing, intensive farming and cultivation on steep slopes, which can lead to slope instability, highlights the importance of remote sensing data as a valuable resource for decision-makers. Based on the spatial relationships between past landslides and their conditioning factors, the assessment and mapping of landslide susceptibility using geospatial technologies enable the prediction and prevention of future landslide occurrences. Landslide susceptibility, which represents the probability of landslide occurrence under specific geological and geomorphological conditions, highlights spatial variations in landslide occurrences and helps to identify areas that are most prone to such events[19].

Geospatial technologies assist decision-makers, scientists and researchers in understanding past landslides and their conditioning factors. These technologies facilitate the assessment and mapping of landslide susceptibility, enabling the prediction and prevention of future landslide occurrences. Storing this information in databases simplifies analysis and facilitates the derivation of actionable insights. This data supports informed planning and management, enabling effective mitigation of such risks. The demarcation of landslide susceptibility zones using GIS software requires the effective extraction of topographic parameters such as slope gradient, slope aspect and plan curvature from digital elevation models (DEMs).

Additionally, it involves evaluating landslide probability based on the hydrogeology and geological conditions of the area, capturing the spatial variation of landslide occurrences and identifying areas most likely to experience such events. Although various modeling approaches using GIS have been widely applied to landslide susceptibility mapping, determining the most effective method for predicting landslide-prone areas remains a challenge.

To address the challenges in landslide-prone regions, the current research focuses on Idukki district in Kerala, India, which is highly susceptible to natural hazards due to its changing climatic conditions and diverse topographical features. The State's location, bordered by the Arabian Sea to the west and the steep slopes of the Western Ghats to the east, further exacerbates its vulnerability to disasters. According to the Kerala State Disaster Management Plan 2016, notable landslides such as the Pettimudi landslide in 2020 and the Kokkayar landslide in 2021 have highlighted the recurring nature of such events. Kerala experiences frequent landslides with debris flows being the most commonly occurring phenomenon. Therefore, assessing landslide susceptibility in the hilly regions of the state is essential for developing effective mitigation strategies to reduce the impact of such disasters.

Landslide susceptibility mapping is crucial for predicting and mitigating landslides, especially in regions prone to natural hazards. Various modeling approaches are employed for this purpose, each offering different strengths and limitations. Deterministic models, for instance, are built upon the mechanisms and processes that govern landslide deformation and failure. These models calculate safety factors using static approaches[10,20,33]. However, they require extensive physical and hydrological data derived from laboratory tests, making them suitable only for small-scale applications[8,13,34]. Despite their accuracy in modeling specific mechanisms, deterministic models often fall short when larger, more diverse data sets are needed across broader landscapes. As a result, their application is often limited to specific sites or smaller regions where such detailed data is available.

In contrast, statistical models offer a more flexible approach by analysing the relationship between past landslides and their conditioning factors through mathematical models[16,22]. These models work with large datasets to determine weighting factors, making them highly adaptable when data is available. However, the reliability of statistical models can be compromised when the dataset is incomplete or lacks sufficient information[39]. Recent advancements have led to the development of several statistical methods such as logistic regression[7,12,31], weights of evidence models[17,30,36,38] and frequency ratio models[5,9,28,41].

Furthermore, data mining techniques including artificial neural networks[6,12,31], support vector machines[4,42]. Decision trees[3,17,18], have also been applied in landslide susceptibility mapping. Among these, the evidential belief function (EBF) model[23,29,35], based on Bayesian theory, has gained popularity for its ability to combine expert knowledge and statistical data, providing robust predictions for landslide zoning. GIS-supported EBF applications have demonstrated effective results in landslide susceptibility assessments, combining both expert input and data-driven models[3,24,33,40].

Study area

The study area is Idukki district in the Western Ghats, Kerala, located between longitude 76°.62′, 77°.41′, latitude 9°.27′, 10°.35′. The district boundaries are Pathanamthitta district in the south, Thrissur in the north, Kottayam district in the west and Tamilnadu in the east. The Idukki district has four taluks, Devikulam, Udubanchola, Peerumade and Thodupuzha. The tallest peak in south India is Anamudi peak situated in the Idukki district with an altitude of 2,694m[11]. This region slopes towards the West, except the Northeast where its slopes towards the East. The major rivers of the district are Thodupuzhayar, Periyar and Thalayar rivers. The district receives an average annual rainfall of about 3,677mm[37]. The maximum temperature ranges from 25.1 to 31.5 °C and the minimum temperature from 18.6 to 14.0 °C.

The major soil types in the Idukki are forest loam, lateritic soils, brown hydromorphic soils and alluvial soils[14]. The predominant landforms in the study area are denudational hills and structural. The district has three major rocks, Peninsular gnessis complex, Charnockite group of rocks and Migmatitic complex. Idukki district, located in Kerala, India, is renowned as the "Spice Garden of Kerala" due to its diverse agricultural activities. The district cultivates a wide range of crops including spices like cardamom, pepper, nutmeg, cinnamon, ginger, turmeric, garlic and cocoa as well as plantation crops such as rubber, tea, coffee and coconut.

Other crops include rice, sugarcane, tapioca, cashew nut, vegetables, tubers and plantains. Its favorable climate and agro-climatic conditions make it ideal for agriculture. Additionally, Idukki is known for its animal husbandry including dairy farming and the rearing of goats, rabbits and pigs. About 50% of the district is covered by reserved forests, the average landholding size is 1.01 hectares and 95% of the landholdings are smaller than 2 hectares.The study area map is represented in the figure 1.

Datasets and Methodology

To generate susceptibility mapping, satellite datasets such as Landsat 8 (30-meter resolution) play a crucial role in preparing land use and land cover (LULC) maps. Landslide magnitude is influenced by various topographical factors including elevation, slope, aspect, profile curvature[32], relief amplitude, slope classifications and indices such as Topographic Wetness Index (TWI), Topographic Position Index (TPI), Terrain Ruggedness Index (TRI), Stream Transport Index (STI) and Stream Power Index (SPI).

Furthermore, open street maps, rainfall data and additional thematic layer datasets acquired from various government websites are incorporated into the study as outlined in table 1 and table 2.

Landslide Conditioning parameters (LCF): The magnitude of landslides in the study area is influenced by a combination of topographical, hydrological, geological and anthropogenic factors.

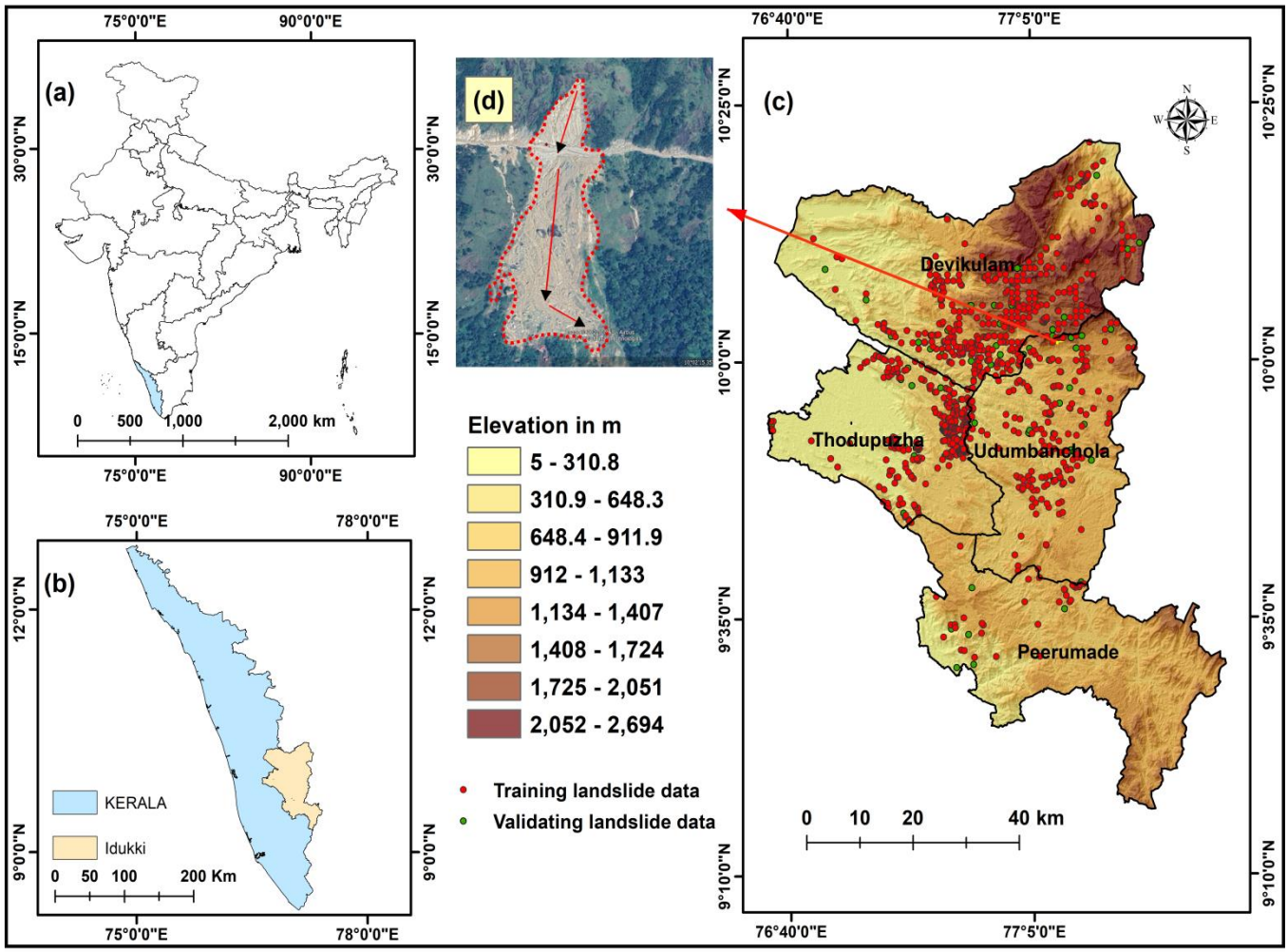

Figure 1: Location Map of the study area: (a) India (b) Kerala (c) Idukki (d) Google Earth image

Table 1
Satellite Data sets used in the landslide susceptibility mapping

S.N.	Satellite Data	Resolution	Description	Sources
1	ASTER DEM	30 meters	Elevation, SPI, STI, TWI, TPI, Slope Aspect, Roughness, Slope classes, Profile Curvature, TRI, Relief Amplitude	https://search.earthdata.nasa.gov
2	Landsat 8	30 meters	Preparation of land use and Land cover mapping and Vegetation mapping of the study area -such as NDVI	https://earthexplorer.usgs.gov

Table 2
Thematic layers datasets

S.N.	Thematic layers	Description	Sources
1	Lithology, Geomorphology, Lineament	Digital lithology, Geomorphology and Lineament thematic maps	https://bhukosh.gsi.gov.in/Bhukosh/MapViewer.aspx
2	Cultural features	Extract the Road network	https://www.openstreetmap.org/
3	Rainfall	Gridded Rainfall data for the annual year 2021 (0.25 X 0.25 Degrees)	https://www.imdpune.gov.in/Clim_Pred_LRF_New/Grided_Data_Download.html

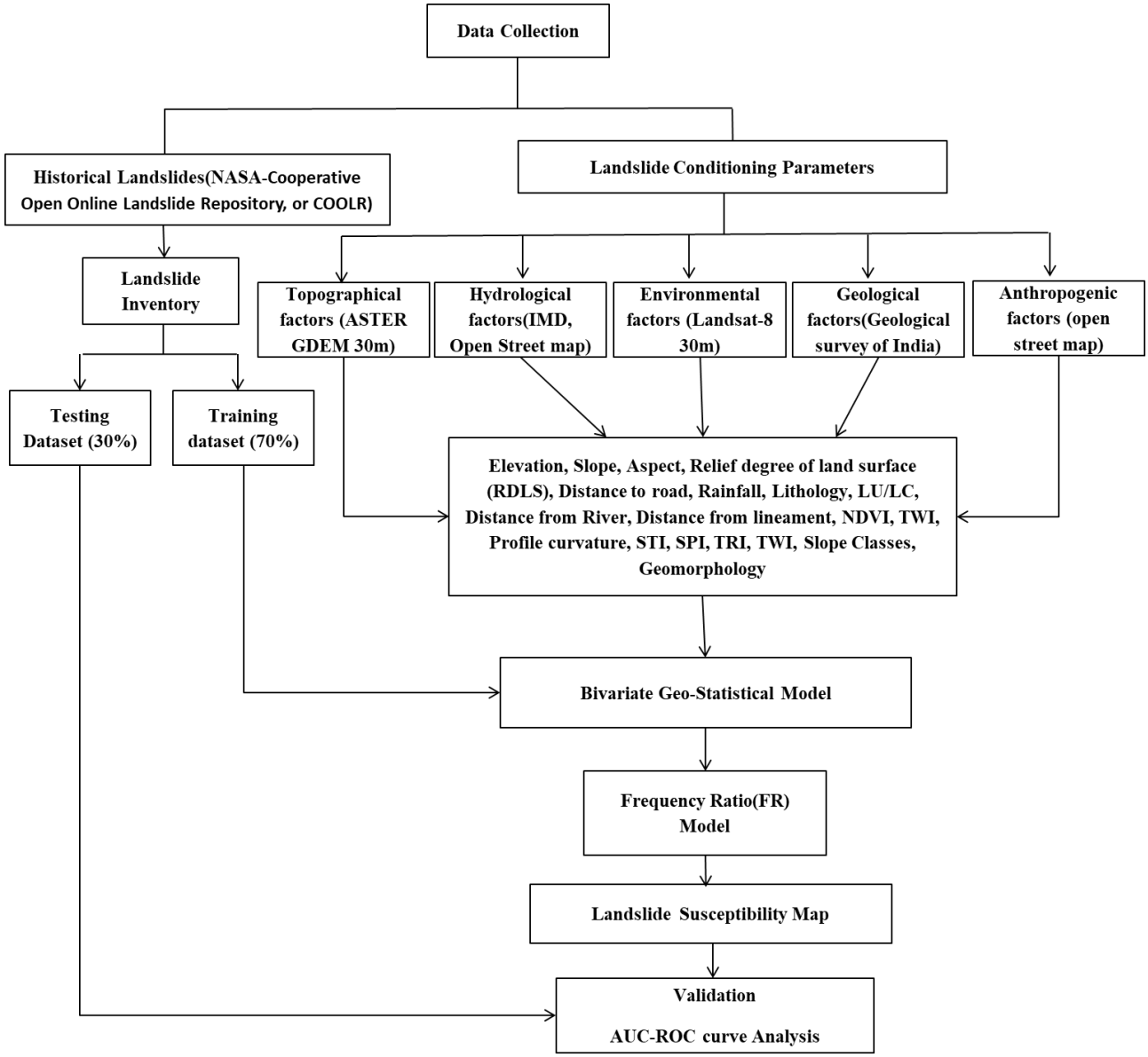

Fig. 2: Methodology

Topographical features are derived from the Digital Elevation Model (DEM) and include parameters such as elevation, slope, aspect, profile curvature, relief amplitude, TRI, TPI, TWI, SPI and STI. Hydrological factors encompass the spatial and temporal patterns of rainfall and the distance to drainage networks. Geological factors include lithology, proximity to lineaments and geomorphology. Anthropogenic factors involve LULC, the assessment of vegetation vigor through the NDVI and the distance to roads.

Landslide Inventory Map: The Landslide inventory map (LIM) is a very important aspect of landslide susceptibility mapping. It helps to recognize the relationship between the distributions of historical landslide locations and selected conditioning factors[2]. In the current study, the inventory data was generated by 1,850 historical landslide points identified from historical records (NASA-Co-operative Open Online Landslide Repository (COOLR) (NASA) and Google Earth dataset.

FR model for Landslide susceptibility mapping: In the present study, landslide susceptibility mapping was produced by employing GIS based Frequency Ratio model using 19 landslide conditioning factors and landslide inventory data. The frequency ratio model[1] is the geospatial calculation tool to assess the probabilistic correlation between the distribution of landslides and each conditioning factor of the landslide[26].

$$Ratio\ of\ area = \frac{number\ of\ class\ pixel}{Total\ no\ of\ class\ pixel} \quad (1)$$

$$Ratio\ of\ Landslide = \frac{number\ of\ Landslide\ \ pixel}{Total\ no\ of\ Landslide\ pixel} \quad (2)$$

$$FR = \frac{Ratio\ of\ landslide}{Ratio\ of\ area} \quad (3)$$

$$Relative\ Frequency(RF) = \frac{FR\ of\ each\ subclass}{Total\ FR\ of\ each\ class} \quad (4)$$

Prediction Rate (PR): The prediction rating of every landslide conditioning factor was calculated using equation

(5)[25]. The frequency ratio model uses relative frequency as input data.

$$PR = \frac{SA_{Max} - SA_{Min}}{Min\,[SA_{Max} - SA_{Min}]} \quad (5)$$

where SA is an indicator of spatial association between conditioning factor and landslides[25]. The maximum, minimum values and frequency ratio values for FR model are in table 3. The Landslide prediction map is shown in figure 3.

Results and Discussion

The present study is to generate the landslide susceptibility map of Idukki district, Kerala using frequency model. The prediction rate values are calculated for all the landslide conditioning factors and are represented in the table 4.

Table 3
Landslide Conditioning Factors for FR Model of Idukki District

S.N.	Factor	Class	Pixel	Landslide occurences	Ratio of Area	Ratio of Landslide	FR	RF
1	Elevation	5 – 450	1059762	90109	0.201	0.093	0.463	0.098
		460-880	1367715	530217	0.259	0.547	2.110	0.447
		890-1300	1845512	184011	0.350	0.190	0.543	0.115
		1400-1800	620434	135637	0.118	0.140	1.190	0.252
		1900-2700	382771	29404	0.073	0.030	0.418	0.089
2	Slope	0-9	1275647	98645	0.242	0.102	0.421	0.087
		0-17	1577640	255149	0.299	0.263	0.880	0.182
		18-25	1346198	357589	0.255	0.369	1.446	0.300
		26-35	836492	233334	0.159	0.241	1.518	0.315
		36-75	240217	24661	0.046	0.025	0.559	0.116
3	Aspect	Flat (-1)	77437	949	0.015	0.001	0.067	0.007
		North (0-22.5)	387875	71138	0.074	0.073	0.998	0.111
		Northeast (22.5-67.5)	705138	167886	0.134	0.173	1.296	0.145
		East (67.5-112.5)	509130	97697	0.096	0.101	1.044	0.117
		Southeast (112.5-157.5)	549479	96748	0.104	0.100	0.958	0.107
		South (157.5-202.5)	733796	152710	0.139	0.158	1.133	0.126
		Southwest (202.5-247.5)	812765	170732	0.154	0.176	1.143	0.128
		West (247.5-292.5)	587244	88211	0.111	0.091	0.818	0.091
		Northwest (292.5-337.5)	588475	74932	0.112	0.077	0.693	0.077
		North (337.5-360)	324855	48374	0.062	0.050	0.810	0.090
4	Profile_curvature	-39.54 - 0	2508799	543497	0.475	0.561	1.179	0.402
		0	305657	52168	0.058	0.054	0.929	0.317
		0.01 - 41.86	2461738	373713	0.467	0.386	0.826	0.282
5	Relief Amplitude	0 - 10	2263585	251355	0.427	0.259	0.607	0.134
		11-20	2134822	513144	0.403	0.529	1.314	0.291
		21-30	702614	182114	0.133	0.188	1.417	0.314
		31-40	147370	18022	0.028	0.019	0.669	0.148
		>40	50797	4743	0.010	0.005	0.510	0.113
6	NDVI	-0.08 - 0.1	121138	10434	0.022	0.011	0.494	0.102
		0.11 - 0.23	683321	164092	0.123	0.169	1.378	0.285
		0.24 - 0.3	1258891	336721	0.226	0.347	1.534	0.317
		0.31 - 0.36	2111956	326288	0.380	0.337	0.886	0.183
		0.37 - 0.93	1385325	131843	0.249	0.136	0.546	0.113
7	SPI	0 - 0.01	1647758	235231	0.312	0.243	0.777	0.188
		0.02 - 99.65	391302	14228	0.074	0.015	0.198	0.048
		99.66- 193.3	221660	31301	0.042	0.032	0.769	0.186
		193.31 - 498.2	649133	130894	0.123	0.135	1.098	0.266
		>498.2	2366341	557724	0.448	0.575	1.283	0.311

8	TWI	2.09 - 8.09	1642019	235231	0.311	0.243	0.780	0.152
		8.1 - 12.42	1526436	332927	0.289	0.343	1.187	0.232
		12.43 - 15.31	1429252	299729	0.271	0.309	1.141	0.223
		15.32 - 19.42	538778	67344	0.102	0.069	0.680	0.133
		19.43 - 30.42	139709	34146	0.026	0.035	1.330	0.260
9	TRI	0 - 92.32	883495	45529	0.167	0.047	0.282	0.066
		92.33 - 184.64	1572655	288347	0.297	0.297	1.002	0.236
		184.65 - 268.57	1695139	463822	0.320	0.478	1.496	0.353
		268.58 - 381.87	906358	146071	0.171	0.151	0.881	0.208
		381.88 - 1,070.08	241541	25610	0.046	0.026	0.580	0.137
10	DTD	0 - 300	1091834	294300	0.196	0.321	1.633	0.373
		301 - 600	977696	189900	0.176	0.207	1.177	0.269
		601-1600	2465091	342900	0.443	0.374	0.843	0.193
		1601-2600	850290	88200	0.153	0.096	0.628	0.144
		2601-5594	175668	2700	0.032	0.003	0.093	0.021
11	STI	0-0.01	1837266	219600	0.348	0.239	0.687	0.235
		0.02-3.69	96186	3600	0.018	0.004	0.215	0.074
		3.7-11.07	148482	9000	0.028	0.010	0.348	0.119
		11.08-22.14	188760	12600	0.036	0.014	0.384	0.131
		>22.15	3005500	673200	0.570	0.733	1.287	0.441
12	TPI	-3.03-0	2736279	570600	0.518	0.622	1.200	0.452
		0-0.01	46327	5400	0.009	0.006	0.671	0.252
		0.01-4.95	2502025	342000	0.473	0.373	0.787	0.296
13	Slope classes	Valleys	895611	168300	0.170	0.183	1.081	0.234
		Upper Slopes	622737	60300	0.118	0.066	0.557	0.121
		Steep Slopes	1597988	255600	0.302	0.278	0.920	0.199
		Ridges	202639	18900	0.038	0.021	0.537	0.116
		Lower Slopes	1884850	411300	0.357	0.448	1.256	0.272
		Gentle Slopes	78844	3600	0.015	0.004	0.263	0.057
14	DTR	0 - 300	2664830	794700	0.479	0.866	1.806	0.656
		301 - 600	745185	89100	0.134	0.097	0.724	0.263
		601-1600	971392	31500	0.175	0.034	0.196	0.071
		1601-2600	358125	900	0.064	0.001	0.015	0.006
		2601-26336	821099	1800	0.148	0.002	0.013	0.005
15	DTL	0 - 300	537596	86400	0.097	0.094	0.974	0.192
		301 - 600	470328	73800	0.085	0.080	0.950	0.188
		601-1600	1353039	241200	0.243	0.263	1.080	0.213
		1601-2600	971441	186300	0.175	0.203	1.162	0.229
		2601-15517	2228227	330300	0.401	0.360	0.898	0.177
16	Lu/Lc	Water	129775	2700	0.023	0.003	0.126	0.024
		Trees	3920434	572400	0.705	0.624	0.884	0.169
		Flooded Vegetation	4548	0	0.001	0.000	0.000	0.000
		Crops	39586	900	0.007	0.001	0.138	0.026
		Built Area	394690	223200	0.071	0.243	3.425	0.653
		bare ground	1071533	118800	0.193	0.129	0.672	0.128
17	RAINFALL	1,116 - 1,837	485144	1800	0.087	0.002	0.022	0.006
		1,838 - 2,558	589223	27900	0.106	0.030	0.287	0.076
		2,559 - 3,280	1256268	319500	0.226	0.348	1.541	0.407
		3,281 - 4,001	2159687	449100	0.388	0.489	1.260	0.333
		4,002 - 4,722	1070309	119700	0.192	0.130	0.677	0.179
18	Lithology	Acid to intermediate charnockite	2296498	122400	0.413	0.133	0.323	0.021
		Banded iron formation	2097	900	0.000	0.001	2.600	0.170
		Biotite gneiss	1052113	351000	0.189	0.382	2.021	0.133
		Calc granulite	484	0	0.000	0.000	0.000	0.000
		Calc granulite with limestone	14522	1800	0.003	0.002	0.751	0.049

		Gar-bio-sill gneiss + graphite + kyanite	26	0	0.000	0.000	0.000	0.000
		Garnet-biotite gneiss	309	0	0.000	0.000	0.000	0.000
		Garnet-sillimanite-gneiss +graphite+cordierite	11	0	0.000	0.000	0.000	0.000
		Granite	57571	18000	0.010	0.020	1.894	0.124
		Hornblende-biotite gneiss	884536	252900	0.159	0.275	1.732	0.114
		Hornblende-diopside gneiss	9	0	0.000	0.000	0.000	0.000
		Hypersthene gneiss?cordierite	202	0	0.000	0.000	0.000	0.000
		Laterite	504	0	0.000	0.000	0.000	0.000
		Pink granite gneiss and Pegamatite	1240008	166500	0.223	0.181	0.813	0.053
		Pyroxene granulite	5003	1800	0.001	0.002	2.179	0.143
		Quartz vein/reef	858	0	0.000	0.000	0.000	0.000
		Quartzite	5568	2700	0.001	0.003	2.937	0.193
19	Geomorphlogy	Dam and Reservoir	128450	3600	0.023	0.004	0.170	0.025
		Flood Plain	222	0	0.000	0.000	0.000	0.000
		Highly Dissected Hills and Valleys	3696919	460800	0.665	0.502	0.755	0.111
		Low Dissected Hills and Valleys	366764	45000	0.066	0.049	0.743	0.109
		Moderately Dissected Hills and Valleys	908213	374400	0.163	0.408	2.497	0.367
		Pediment Pediplain Complex	417062	18900	0.075	0.021	0.274	0.040
		Waterbodies-Other	3403	0	0.001	0.000	0.000	0.000
		Waterbody - River	39286	15300	0.007	0.017	2.359	0.347

Table 4
Prediction rate (PR) of FR

Factors	**FR**			
	SA_Max	**SA_Min**	**l SA_Max -SA_Min l**	**PR_FR**
Elevation	0.447	0.089	0.358	6.876
Slope	0.315	0.087	0.227	4.367
Slope_Aspect	0.145	0.007	0.137	2.633
Profile_curvature	0.402	0.282	0.120	2.308
Relief Amplitude	0.314	0.113	0.201	3.853
NDVI	0.317	0.102	0.215	4.128
SPI	0.311	0.048	0.263	5.051
TWI	0.260	0.133	0.127	2.438
TRI	0.353	0.066	0.286	5.496
DTD	0.373	0.021	0.352	6.759
STI	0.441	0.074	0.367	7.046
TPI	0.452	0.252	0.199	3.823
Slope classes	0.272	0.057	0.215	4.131
DTR	0.656	0.005	0.651	12.492
DTL	0.229	0.177	0.052	1.000
LULC	0.653	0.000	0.653	12.537
RAINFALL	0.407	0.006	0.401	7.696
Lithology	0.193	0.000	0.193	3.698
Geomorphology	0.367	0.000	0.367	7.051

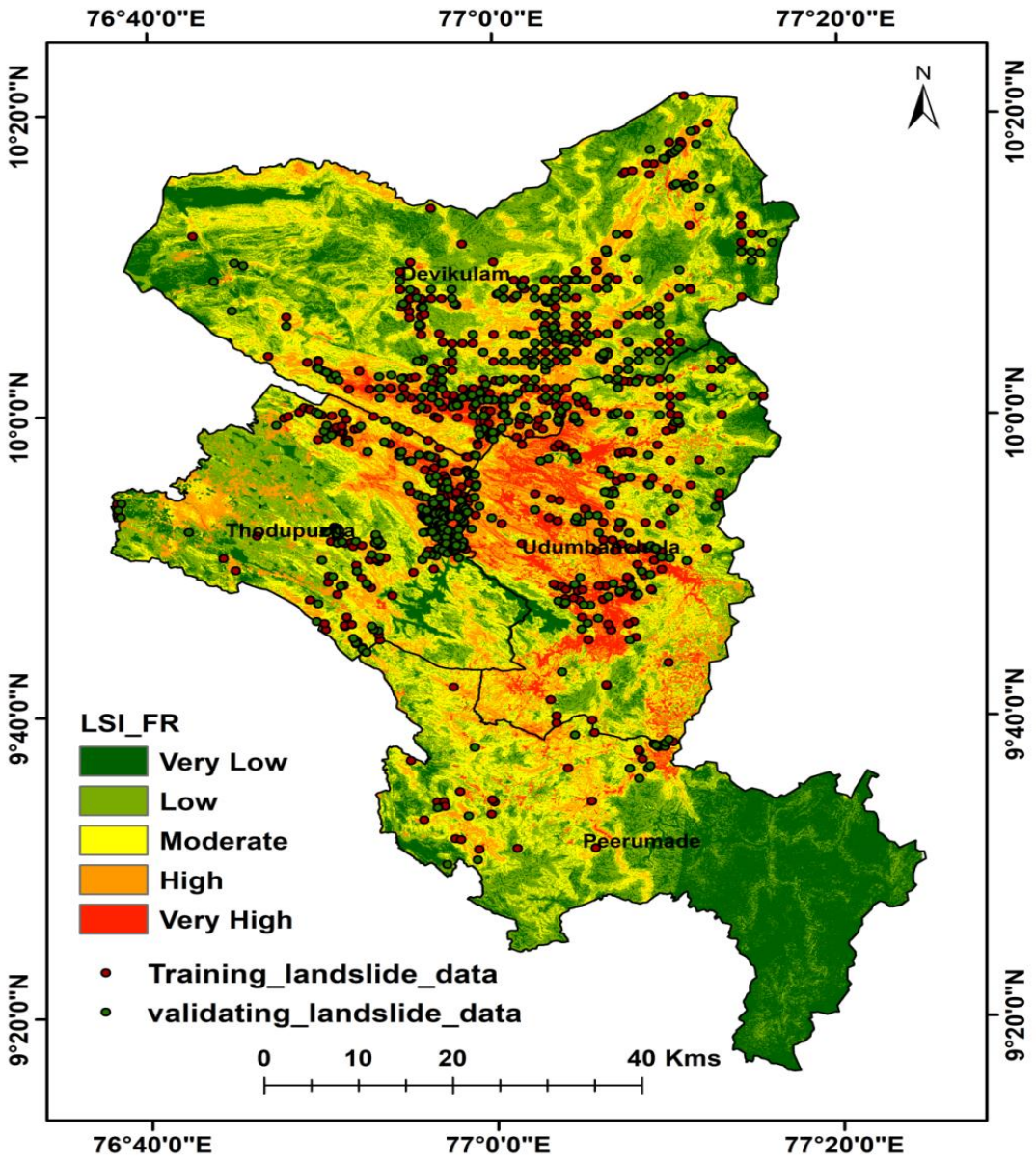

Figure 3: Landslide prediction map for Frequency Ratio model

Table 5
Percentage of area of FR model for landslide prediction

Susceptibility class	Area in sqkm	Area in %
Very low	960.90	19.24
Low	1463.99	29.31
Medium	1365.01	27.33
High	893.97	17.90
Very high	310.69	6.22

The prediction rate (PR) of frequency ratio (FR) analysis highlights the influence of various conditioning factors on land susceptibility, with Land Use Land Cover (LULC) (PR_FR = 12.537) and Distance to River (DTR) (PR_FR = 12.492) emerging as the most significant contributors. The high susceptibility linked to LULC suggests that anthropogenic activities such as deforestation and urban expansion, play a crucial role in destabilizing slopes. Similarly, proximity to rivers increases the likelihood of erosion and soil saturation, leading to higher susceptibility. Other key factors such as rainfall (PR_FR = 7.696), geomorphology (PR_FR = 7.051), standardized topographic index (STI) (PR_FR = 7.046) and elevation (PR_FR = 6.876), also exhibit strong predictive capabilities. These findings align with existing research, emphasizing the impact of hydrological and topographic conditions on land susceptibility. Additionally, parameters like Distance to Drainage (DTD) (PR_FR = 6.759), Topographic Roughness

Index (TRI) (PR_FR = 5.496) and Stream Power Index (SPI) (PR_FR = 5.051) reinforce the importance of terrain characteristics in determining susceptibility levels.

In contrast, factors such as Slope Aspect (PR_FR = 2.633), Topographic Wetness Index (TWI) (PR_FR = 2.438) and Distance to Landslide (DTL) (PR_FR = 1.000) exhibit lower prediction rates, indicating a relatively minor influence on susceptibility. Moderate contributors include lithology (PR_FR = 3.698), slope (PR_FR = 4.367) and NDVI (PR_FR = 4.128), which impact soil stability and vegetation cover. The results suggest that land susceptibility mapping should prioritize high-impact factors such as LULC, rainfall, geomorphology and elevation, which exhibit stronger correlations with land susceptibility. These insights can be instrumental in guiding disaster mitigation strategies, sustainable land-use planning and environmental risk assessments, ensuring a data-driven approach to land management.

From table 5, the GSFR model for landslide prediction categorizes the study area into five susceptibility classes: very low, low, medium, high and very high, based on the percentage of land coverage. The largest proportion of the area falls under the low susceptibility class (29.31%), covering 1463.99 sq. km. followed by the medium susceptibility class (27.33%) and accounting for 1365.01 sq. km. These findings indicate that a significant portion of the region experiences moderate to low landslide risk where occasional instability may occur due to specific triggering factors such as heavy rainfall or anthropogenic influences. The very low susceptibility zone covers 960.90 sq. km. (19.24%) representing stable terrain with minimal chances of landslides, often located in areas with gentle slopes and dense vegetation.

In contrast, the high susceptibility zone spans 893.97 sq. km. (17.90%), highlighting regions where landslide occurrences are relatively frequent, likely influenced by steep slopes, weak lithology, or hydrological factors. The very high susceptibility class, covering the smallest area of 310.69 sq. km. (6.22%) represents the most critical regions where landslides are highly probable. These areas may require urgent monitoring and mitigation measures, as they pose significant risks to infrastructure, settlements and human life. The spatial distribution of susceptibility levels suggests that targeted intervention strategies should focus on high-risk zones while promoting sustainable land-use planning in medium and low-susceptibility areas to prevent future hazards.

Validation: Validation of landslide-susceptible zones is the most important step in the whole process. Without validation the results will have no scientific significance. In the present study, the LSZ map is produced by the FR model and is validated by comparing the susceptibility map with training data (70%) and testing data (30%). The ROC-AUC method is used to calculate the success and prediction rates of landslide susceptibility. The success rate accuracy of LSZ maps was obtained by comparing the landslide point training data (70%) in figure 4a. The results presented that a success rate is 0.827 was obtained. Similarly, the prediction rate accuracy was obtained by comparing the testing data (30%) shown in figure 4b. The results showed that the prediction rate is 0.835 obtained. Through the technical analysis, the FR model achieved excellent accuracy in landslide susceptibility mapping in the study area.

Conclusion

The Western Ghats region of India faces a large number of landslide incidents causing huge losses to humans and the environment. In this study, a GIS-based FR model is used to predict the landslide-susceptible zones in the Idukki district, Kerala, India. To produce a susceptibility map of the landslide, 19 conditioning parameters are considered and prepared using the ArcGIS Platform. The landslide susceptibility using the FR model is cross-validated by using the ROC-AUC method. FR model exhibits higher accuracy in both the success and prediction rates.

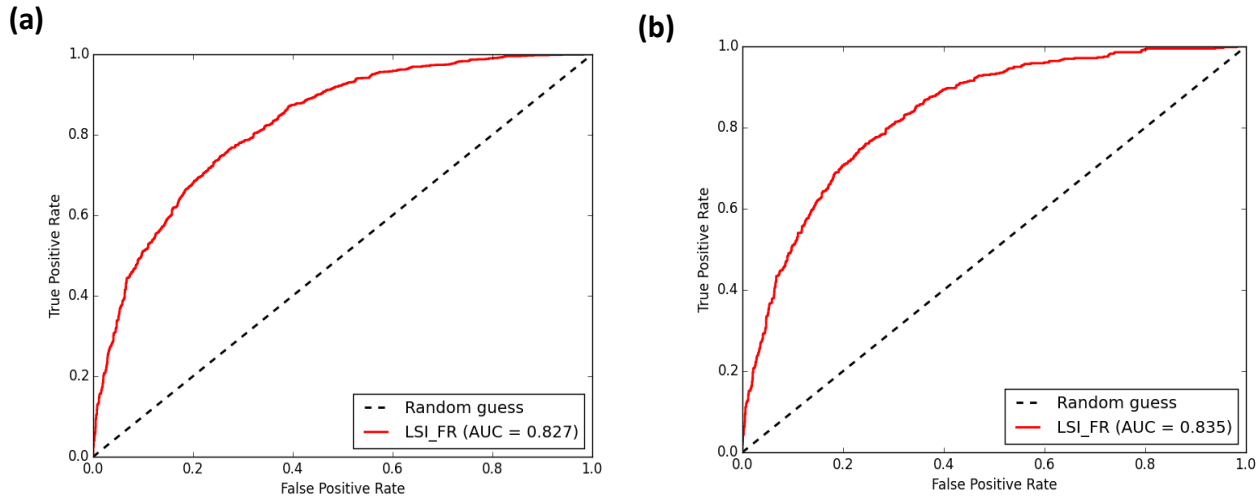

Figure 4: The success and prediction rate for Landslide susceptibility map (a) Success rate (b) Prediction rate.

The susceptibility zones are categorized into five classes through the natural break method: Very low, Low, Moderate, High and Very High each covering an area of 19.24%, 29.31%, 27.33%, 17.90% and 6.22% respectively in the study area. According to the results, the distance to road and LU/LC conditioning factors have strong association with landslide occurrence, with high prediction rate. Based on these findings, it is recommended to identify high and very high-risk zones and take mitigation measures to reduce the impact of the landslide event in the study area.

References

1. Abdo H.G., Assessment of landslide susceptibility zonation using frequency ratio and statistical index: A case study of Al-Fawar basin, Tartous, Syria, *International Journal of Environmental Science and Technology*, **19(4)**, 2599–2618, https://doi.org/10.1007/s13762-021-03322-1 **(2022)**

2. Ali S.A., Parvin F., Vojteková J., Costache R., Linh N.T.T., Pham Q.B., Vojtek M., Gigović L., Ahmad A. and Ghorbani M.A., GIS-based landslide susceptibility modeling: A comparison between fuzzy multi-criteria and machine learning algorithms, *Geoscience Frontiers*, **12(2)**, 857–876, https://doi.org/10.1016/j.gsf.2020.09.004 **(2021)**

3. Althuwaynee O.F., Pradhan B. and Lee S., Application of an evidential belief function model in landslide susceptibility mapping, *Computers & Geosciences*, **44**, 120–135 **(2012)**

4. Ballabio C. and Sterlacchini S., Support Vector Machines for Landslide Susceptibility Mapping: The Staffora River Basin Case Study, Italy, *Mathematical Geosciences*, **44(1)**, 47–70, https://doi.org/10.1007/s11004-011-9379-9 **(2012)**

5. Barman J. and Das J., Assessing classification system for landslide susceptibility using frequency ratio, analytical hierarchical process and geospatial technology mapping in Aizawl district, NE India, *Advances in Space Research*, **74(3)**, 1197–1224, https://doi.org/10.1016/j.asr.2024.05.007 **(2024)**

6. Bragagnolo L., Da Silva R.V. and Grzybowski J.M.V., Landslide susceptibility mapping with r.landslide: A free open-source GIS-integrated tool based on Artificial Neural Networks, *Environmental Modelling & Software*, **123**, 104565, https://doi.org/10.1016/j.envsoft.2019.104565 **(2020)**

7. Chen W., Pourghasemi H.R., Kornejady A. and Zhang N., Landslide spatial modeling: Introducing new ensembles of ANN, MaxEnt and SVM machine learning techniques, *Geoderma*, **305**, 314–327, https://doi.org/10.1016/j.geoderma.2017.06.020 **(2017)**

8. Dai F.C. and Lee C.F., Landslide characteristics and slope instability modeling using GIS, Lantau Island, Hong Kong, *Geomorphology*, **42(3–4)**, 213–228, https://doi.org/10.1016/S0169-555X(01)00087-3 **(2002)**

9. Das J., Saha P., Mitra R., Alam A. and Kamruzzaman M., GIS-based data-driven bivariate statistical models for landslide susceptibility prediction in Upper Tista Basin, India, *Heliyon*, **9(5)**, e16186, https://doi.org/10.1016/j.heliyon.2023.e16186 **(2023)**

10. Dietrich W.E., Reiss R., Hsu M. and Montgomery D.R., A process-based model for colluvial soil depth and shallow landsliding using digital elevation data, *Hydrological Processes*, **9(3–4)**, 383–400, https://doi.org/10.1002/hyp.3360090311 **(1995)**

11. Directorate of Census Operations, Kerala, District Census Handbook—Idukki, Series 33—Part XII B, (CENSUS Series 33-Part XII B, District Census Handbook, Idukki), Census of India **(2011)**

12. Dou J., Yamagishi H., Pourghasemi H.R., Yunus A.P., Song X., Xu Y. and Zhu Z., An integrated artificial neural network model for the landslide susceptibility assessment of Osado Island, Japan, *Natural Hazards*, **78(3)**, 1749–1776 **(2015)**

13. Gómez H. and Kavzoglu T., Assessment of shallow landslide susceptibility using artificial neural networks in Jabonosa River Basin, Venezuela, *Engineering Geology*, **78(1–2)**, 11–27, https://doi.org/10.1016/j.enggeo.2004.10.004 **(2005)**

14. Government of Kerala, District Survey Report of minor minerals.pdf, Department of Mining and Geology **(2016)**

15. Gulbet E. and Getahun B., Landslide susceptibility mapping using frequency ratio and analytical hierarchy process method in Awabel Woreda, Ethiopia, *Quaternary Science Advances*, **16**, 100246, https://doi.org/10.1016/j.qsa.2024.100246 **(2024)**

16. Hadmoko D.S., Lavigne F. and Samodra G., Application of a semiquantitative and GIS-based statistical model to landslide susceptibility zonation in Kayangan Catchment, Java, Indonesia, *Natural Hazards*, **87(1)**, 437–468, https://doi.org/10.1007/s11069-017-2772-z **(2017)**

17. Hong H., Liu J., Bui D.T., Pradhan B., Acharya T.D., Pham B.T., Zhu A.X., Chen W. and Ahmad B.B., Landslide susceptibility mapping using J48 Decision Tree with AdaBoost, Bagging and Rotation Forest ensembles in the Guangchang area (China), *CATENA*, **163**, 399–413, https://doi.org/10.1016/j.catena.2018.01.005 **(2018)**

18. Hong H., Pradhan B., Sameen M.I., Chen W. and Xu C., Spatial prediction of rotational landslide using geographically weighted regression, logistic regression and support vector machine models in Xing Guo area (China), *Geomatics, Natural Hazards and Risk*, **8(2)**, 1997–2022 **(2017)**

19. Ilia I. and Tsangaratos P., Applying weight of evidence method and sensitivity analysis to produce a landslide susceptibility map, *Landslides*, **13(2)**, 379–397, https://doi.org/10.1007/s10346-015-0576-3 **(2016)**

20. Intarawichian N. and Dasananda S., Frequency ratio model based landslide susceptibility mapping in lower Mae Chaem watershed, Northern Thailand, *Environmental Earth Sciences*, **64(8)**, 2271–2285, https://doi.org/10.1007/s12665-011-1055-3 **(2011)**

21. Kallungal D., Human interventions, excessive rain have combined effect on landslides, reveal post-disaster studies, *The Hindu*, https://www.thehindu.com/news/national/kerala/human-interventions-excessive-rain-have-combined-effect-on-landslides-reveal-post-disaster-studies/article68513365.ece **(2024)**

22. Komac M., A landslide susceptibility model using the Analytical Hierarchy Process method and multivariate statistics in

perialpine Slovenia, *Geomorphology*, **74(1–4)**, 17–28, https://doi.org/10.1016/j.geomorph.2005.07.005 **(2006)**

23. Laxmi Ch. N.V. and Kumari K.P., Evidential Belief Function (EBF) Model for Landslide Susceptibility Analysis in Idukki District, Kerala, India, *International Journal of Environment and Climate Change*, **14(12)**, 464–472, https://doi.org/10.9734/ijecc/2024/v14i124637 **(2024)**

24. Lee S., Hwang J. and Park I., Application of data-driven evidential belief functions to landslide susceptibility mapping in Jinbu, Korea, *Catena*, **100**, 15–30 **(2013)**

25. Meena S.R., Puliero S., Bhuyan K., Floris M. and Catani F., Assessing the importance of conditioning factor selection in landslide susceptibility for the province of Belluno (region of Veneto, northeastern Italy), *Natural Hazards and Earth System Sciences*, **22(4)**, 1395–1417, https://doi.org/10.5194/nhess-22-1395-2022 **(2022)**

26. Mehrabi M., Pradhan B., Moayedi H. and Alamri A., Optimizing an adaptive neuro-fuzzy inference system for spatial prediction of landslide susceptibility using four state-of-the-art metaheuristic techniques, *Sensors*, **20(6)**, 1723 **(2020)**

27. Mersha T. and Meten M., GIS-based landslide susceptibility mapping and assessment using bivariate statistical methods in Simada area, northwestern Ethiopia, *Geoenvironmental Disasters*, **7(1)**, 20, https://doi.org/10.1186/s40677-020-00155-x **(2020)**

28. Mohammady M., Pourghasemi H.R. and Pradhan B., Landslide susceptibility mapping at Golestan Province, Iran: A comparison between frequency ratio, Dempster–Shafer and weights-of-evidence models, *Journal of Asian Earth Sciences*, **61**, 221–236, https://doi.org/10.1016/j.jseaes.2012.10.005 **(2012)**

29. Mondal S. and Mandal S., Data-driven evidential belief function (EBF) model in exploring landslide susceptibility zones for the Darjeeling Himalaya, India, *Geocarto International*, **35(8)**, 818–856, https://doi.org/10.1080/10106049.2018.1544288 **(2020)**

30. Neuhäuser B., Damm B. and Terhorst B., GIS-based assessment of landslide susceptibility on the base of the Weights-of-Evidence model, *Landslides*, **9(4)**, 511–528, https://doi.org/10.1007/s10346-011-0305-5 **(2012)**

31. Nourani V., Pradhan B., Ghaffari H. and Sharifi S.S., Landslide susceptibility mapping at Zonouz Plain, Iran using genetic programming and comparison with frequency ratio, logistic regression and artificial neural network models, *Natural Hazards*, **71(1)**, 523–547, https://doi.org/10.1007/s11069-013-0932-3 **(2014)**

32. Poddar I. and Roy R., Application of GIS-based data-driven bivariate statistical models for landslide prediction: A case study of highly affected landslide prone areas of Teesta River basin, *Quaternary Science Advances*, **13**, 100150, https://doi.org/10.1016/j.qsa.2023.100150 **(2024)**

33. Pradhan A.M.S. and Kim Y.T., Evaluation of a combined spatial multi-criteria evaluation model and deterministic model for landslide susceptibility mapping, *CATENA*, **140**, 125–139, https://doi.org/10.1016/j.catena.2016.01.022 **(2016)**

34. Regmi R.K., Jung K., Nakagawa H. and Kang J., Study on mechanism of retrogressive slope failure using artificial rainfall, *CATENA*, **122**, 27–41, https://doi.org/10.1016/j.catena.2014.06.001 **(2014)**

35. Roy D., Sarkar A., Kundu P., Paul S. and Chandra Sarkar B., An ensemble of evidence belief function (EBF) with frequency ratio (FR) using geospatial data for landslide prediction in Darjeeling Himalayan region of India, *Quaternary Science Advances*, **11**, 100092, https://doi.org/10.1016/j.qsa.2023.100092 **(2023)**

36. Sahana M. and Sajjad H., Evaluating effectiveness of frequency ratio, fuzzy logic and logistic regression models in assessing landslide susceptibility: A case from Rudraprayag district, India, *Journal of Mountain Science*, **14(11)**, 2150–2167, https://doi.org/10.1007/s11629-017-4404-1 **(2017)**

37. Singadurai S., Ground water information booklet of Idukki District, Kerala State, Thiruvananthapuram **(2013)**

38. Sujatha E.R. and Sridhar V., Landslide Susceptibility Analysis: A Logistic Regression Model Case Study in Coonoor, India, *Hydrology*, **8(1)**, 41, https://doi.org/10.3390/hydrology8010041 **(2021)**

39. Thiery Y., Malet J.P., Sterlacchini S., Puissant A. and Maquaire O., Landslide susceptibility assessment by bivariate methods at large scales: Application to a complex mountainous environment, *Geomorphology*, **92(1–2)**, 38–59, https://doi.org/10.1016/j.geomorph.2007.02.020 **(2007)**

40. Tien Bui D., Tuan T.A., Klempe H., Pradhan B. and Revhaug I., Spatial prediction models for shallow landslide hazards: A comparative assessment of the efficacy of support vector machines, artificial neural networks, kernel logistic regression and logistic model tree, *Landslides*, **13(2)**, 361–378, https://doi.org/10.1007/s10346-015-0557-6 **(2016)**

41. Yalcin A., Reis S., Aydinoglu A.C. and Yomralioglu T., A GIS-based comparative study of frequency ratio, analytical hierarchy process, bivariate statistics and logistics regression methods for landslide susceptibility mapping in Trabzon, NE Turkey, *CATENA*, **85(3)**, 274–287, https://doi.org/10.1016/j.catena.2011.01.014 **(2011)**

42. Yao X., Tham L.G. and Dai F.C., Landslide susceptibility mapping based on Support Vector Machine: A case study on natural slopes of Hong Kong, China, *Geomorphology*, **101(4)**, 572–582, https://doi.org/10.1016/j.geomorph.2008.02.011 **(2008)**.

(Received 14th March 2025, accepted 16th May 2025)